GEOPHYSICS, VOL. 74, NO. 1 (JANUARY-FEBRUARY 2009); P. T1–T11, 7 FIGS., 1 TABLE.
10.1190/1.3008548

Theory and modeling of constant-*Q* P- and S-waves using fractional time derivatives

José M. Carcione[1]

ABSTRACT

I have developed and solved the constant-Q model for the attenuation of P- and S-waves in the time domain using a new modeling algorithm based on fractional derivatives. The model requires time derivatives of order $m + 2\gamma$ applied to the strain components, where $m = 0,1,\ldots$ and $\gamma = (1/\pi)\tan^{-1}(1/Q)$, with Q the P-wave or S-wave quality factor. The derivatives are computed with the Grünwald-Letnikov and central-difference fractional approximations, which are extensions of the standard finite-difference operators for derivatives of integer order. The modeling uses the Fourier method to compute the spatial derivatives, and therefore can handle complex geometries and general material-property variability. I verified the results by comparison with the 2D analytical solution obtained for wave propagation in homogeneous Pierre Shale. Moreover, the modeling algorithm was used to compute synthetic seismograms in heterogeneous media corresponding to a crosswell seismic experiment.

INTRODUCTION

Constant-Q models provide an efficient parameterization of seismic attenuation in rocks. By reducing the number of parameters, they allow an improvement of seismic inversion. Moreover, there is physical evidence that attenuation is almost linear with frequency (therefore Q is constant) in many frequency bands (e.g., McDonal et al., 1958). Bland (1960) and Kjartansson (1979) discuss a linear attenuation model with the required characteristics, but the idea is much older (Scott-Blair, 1949). Kjartansson's constant-Q model is based on a creep function of the form $t^{2\gamma}$, where t is time and $\gamma \ll 1$ for seismic applications. This model is completely specified by two parameters, i.e., the phase velocity at a reference frequency and Q. Therefore, it is mathematically much simpler than any model with nearly constant Q, as, for instance, a spectrum of Zener models (e.g., Carcione, 2007). Because of its simplicity, Kjartansson's model is used in many seismic applications, mainly in its frequency-domain form. Mainardi and Tomirotti (1997) interpret the constant-Q model in terms of fractional derivatives and obtained its 1D Green's function. The wave equation becomes parabolic because the phase velocity has no upper bound.

Seismic modeling in inhomogeneous media can, in principle, be performed in the frequency domain. However, the method is expensive when using differential formulations, because it involves solution of many Helmholtz equations. The alternative is to compute the solution through a time-convolution, but the resulting algorithm is relatively expensive. A purely differential — as opposed to integro-differential — formulation can be obtained by using fractional derivatives (Caputo and Mainardi, 1971; Hanyga, 2002).

Fractional derivatives appear also in Biot theory, related to memory effects in porous rocks at seismic frequencies with $\gamma = 1/4$ (Gurevich and Lopatnikov, 1995; Lu and Hanyga, 2005) and at low- and high-frequency limits (Fellah and Depollier, 2000). Fractional derivatives can be computed with the Grünwald-Letnikov (GL) and central-difference (CD) approximations, which are extensions of the standard finite-difference (FD) approximation for derivatives of integer order (Grünwald, 1867; Letnikov, 1868; Gorenflo, 1997). Unlike the standard operator of differentiation, the fractional operator increases in length as time increases, because it must keep the memory effects. However, after a given time period the operator can be truncated (short memory principle).

The case of P-wave propagation has been solved by Carcione et al. (2002). Instead of time derivatives of order 2, they use derivatives of order $2 - 2\gamma$ with $0 < \gamma < 1/2$ in the dilatation formulation of the wave equation, and order 2γ in the dilatation-stress formulation. Here, I extend the theory and the algorithm to model the propagation and attenuation of P- and S-waves. In the first part of this work, I review the constant-Q model and calculate the complex moduli, phase velocities, and attenuation factors versus frequency. I then recast the viscoelastic wave equation in the time domain in terms of fractional derivatives, and obtain the GL and CD approximations. Then, I veri-

Manuscript received by the Editor 2 May 2008; revised manuscript received 24 July 2008; published online 12 December 2008.
[1]Istituto Nazionale di Oceanografia e di Geofisica Sperimentale, Trieste, Italy. E-mail: jcarcione@ogs.trieste.it.

fy the accuracy of the time discretization by comparing the exact and the FD phase velocities and attenuation factors. The model is discretized on a mesh, and the spatial derivatives are calculated with the Fourier method by using the fast Fourier transform. This approximation is infinitely accurate for band-limited periodic functions with cutoff spatial wavenumbers smaller than the cutoff wavenumbers of the mesh. Finally, I test the modeling algorithms with an analytical solution for a 2D homogeneous medium, and illustrate the method with seismic modeling in inhomogeneous media.

DYNAMICAL EQUATIONS

The conservation of linear momentum for a linear anelastic medium can be written as

$$\partial_j \sigma_{ij} + f_i = \rho \partial_{tt}^2 u_i \tag{1}$$

(Auld, 1990), where σ_{ij} are the components of the stress tensor ($i,j = 1,\ldots,3$), u_i are the components of the displacement vector, ρ is the mass density, and f_i are the components of the body forces per unit volume. Summation over repeated indices is assumed in equation 1.

The initial conditions are

$$u_i(0,\mathbf{x}) = \partial_t u_i(0,\mathbf{x}) = 0, \quad u_i(t,\mathbf{x}) = 0, \quad \text{for } t < 0, \tag{2}$$

where $\mathbf{x}$ is the position vector. Moreover, the source function satisfies the condition

$$f_i(t,\mathbf{x}) = 0, \quad \text{for } t \leq 0. \tag{3}$$

I introduce the constitutive relation

$$\sigma_{ij} = \psi_{ijkl} * \partial_t \epsilon_{kl}, \tag{4}$$

where $*$ denotes time convolution, ψ_{ijkl} are the components of the relaxation tensor, and ϵ_{kl} are the components of the strain tensor, which can be obtained in terms of the displacement components as

$$\epsilon_{kl} = \frac{1}{2}(\partial_k u_l + \partial_l u_k). \tag{5}$$

The most general isotropic representation of the fourth-order relaxation tensor is

$$\psi_{ijkl}(t) = [\mathcal{E}(t) - 2\mu(t)]\delta_{ij}\delta_{kl} + \mu(t)(\delta_{ik}\delta_{jl} + \delta_{il}\delta_{jk}) \tag{6}$$

(Christensen, 1982), where $\mathcal{E}$ and μ are independent relaxation functions. They correspond to the P-wave modulus $\mathcal{E} = \lambda + 2\mu$ and the rigidity modulus μ, where λ and μ are the Lamé constants in lossless media. For clarity, I keep the same notation for the relaxation functions.

Substituting equation 6 into the constitutive equation 4 gives

$$\sigma_{ij} = \mathcal{E}(t) * \partial_t \epsilon_{kk}\delta_{ij} + 2\mu(t) * [\partial_t \epsilon_{ij} - \partial_t \epsilon_{kk}\delta_{ij}]. \tag{7}$$

Constant-Q model

Let us denote a stress component of the isotropic stress-strain relation 7 by σ and the strain components by ϵ. Each term in equation 7 has the form

$$\sigma(t) = \psi(t) * \partial_t \epsilon(t), \tag{8}$$

where ψ is the relaxation function representing $\mathcal{E}$ or μ.

Kjartansson's model of constant Q assumes (Caputo and Mainardi, 1971; Kjartansson, 1979; Carcione et al., 2002)

$$\psi(t) = \frac{M_0}{\Gamma(1-2\gamma)}\left(\frac{t}{t_0}\right)^{-2\gamma} H(t), \tag{9}$$

where M_0 is a bulk modulus, Γ is Euler's Gamma function, t_0 is a reference time, γ is a dimensionless parameter, and H is the Heaviside step function. The parameters M_0, t_0, and γ have precise physical meanings, which will become clear in the following analysis. Implementing relaxation functions such as equation 9 in seismic modeling requires that at each step one has to perform a time integration (convolution), which is more computationally expensive than introducing additional field variables (Carcione et al., 1988). In addition, in this case (a constant-Q power-law), one has to deal with $1/t$ singularities. Therefore, a purely differential formulation based on fractional derivatives is used to limit the number of computations.

The Fourier transform of equation 8 is

$$\tilde{\sigma}(\omega) = \mathcal{F}(\partial_t \psi(t))\tilde{\epsilon}(\omega) \equiv M(\omega)\tilde{\epsilon}(\omega), \tag{10}$$

where $\mathcal{F}$ is the Fourier transform operator, $M(\omega)$ is the complex modulus, and the tilde denotes the Fourier transform. For Kjartansson's model,

$$M(\omega) = M_0\left(\frac{\mathrm{i}\omega}{\omega_0}\right)^{2\gamma}, \tag{11}$$

where $\mathrm{i} = \sqrt{-1}$, and $\omega_0 = 1/t_0$ is the reference frequency. It is shown in Kjartansson (1979) and Carcione et al. (2002) that the quality factor associated with the complex modulus M is

$$Q = \frac{\mathrm{Re}(M)}{\mathrm{Im}(M)} = \frac{1}{\tan(\pi\gamma)}. \tag{12}$$

Moreover, the bulk modulus M_0 is related to the reference wave velocity c_0 by the formula

$$M_0 = \rho c_0^2 \cos^2\left(\frac{\pi\gamma}{2}\right). \tag{13}$$

It follows from equation 12 that Q is independent of frequency, so that

$$\gamma = \frac{1}{\pi}\tan^{-1}\left(\frac{1}{Q}\right) \tag{14}$$

parameterizes the attenuation level. Hence, $Q > 0$ is equivalent to $0 < \gamma < 1/2$.

Constitutive equation with fractional derivatives

The convolutional constitutive equation 8 can be calculated in terms of fractional derivatives (Caputo and Mainardi, 1971; Podlubny, 1999). It is equivalent to

$$\sigma = CD^{2\gamma}\epsilon, \tag{15}$$

where $D^{2\gamma}$ is the time fractional derivative of order 2γ,

$$C = M_0\omega_0^{-2\gamma}. \tag{16}$$

In terms of fractional derivatives, the constitutive equation 7 becomes

$$\sigma_{ij} = C_{\mathcal{E}} D^{2\gamma_P} \epsilon_{kk} \delta_{ij} + 2C_{\mu} D^{2\gamma_S} (\epsilon_{ij} - \epsilon_{kk} \delta_{ij}), \quad (17)$$

where

$$C_{\mathcal{E}} = \mathcal{E}_0 \omega_0^{-2\gamma_P}, \quad C_{\mu} = \mu_0 \omega_0^{-2\gamma_S}, \quad (18)$$

with $\mathcal{E}_0$ and μ_0 the reference moduli, defined at the same reference frequency ω_0, and

$$\gamma_P = \frac{1}{\pi} \tan^{-1}\left(\frac{1}{Q_P}\right), \quad \gamma_S = \frac{1}{\pi} \tan^{-1}\left(\frac{1}{Q_S}\right), \quad (19)$$

where Q_P and Q_S are the P-wave and S-wave quality factors, respectively. The moduli $\mathcal{E}_0$ and μ_0 can be expressed in terms of the P-wave and S-wave velocities c_P and c_S as

$$\mathcal{E}_0 = \rho c_P^2 \cos^2\left(\frac{\pi \gamma_P}{2}\right) \text{ and } \mu_0 = \rho c_S^2 \cos^2\left(\frac{\pi \gamma_S}{2}\right) \quad (20)$$

(see equation 13).

Phase velocities and attenuation factors

The complex wave velocities can be obtained in terms of the complex moduli as

$$V_P = \sqrt{\frac{\mathcal{E}(\omega)}{\rho}} \text{ and } V_S = \sqrt{\frac{\mu(\omega)}{\rho}}. \quad (21)$$

The dynamic moduli $\mathcal{E}$ and μ are given by equation 11, viz.,

$$\mathcal{E}(\omega) = \mathcal{E}_0 \left(\frac{i\omega}{\omega_0}\right)^{2\gamma_P}, \text{ and } \mu(\omega) = \mu_0 \left(\frac{i\omega}{\omega_0}\right)^{2\gamma_S}. \quad (22)$$

The phase velocity is the frequency ω divided by the real part of the complex wavenumber (ω/V_P and ω/V_S, respectively). Then,

$$c_{\text{phase}}^P = \left[\text{Re}\left(\frac{1}{V_P}\right)\right]^{-1} \text{ and } c_{\text{phase}}^S = \left[\text{Re}\left(\frac{1}{V_S}\right)\right]^{-1}. \quad (23)$$

They simply become

$$c_{\text{phase}}^P = c_P \left|\frac{\omega}{\omega_0}\right|^{\gamma_P} \text{ and } c_{\text{phase}}^S = c_S \left|\frac{\omega}{\omega_0}\right|^{\gamma_S}. \quad (24)$$

The attenuation factors are given by

$$\alpha_P = -\omega \,\text{Im}\left(\frac{1}{V_P}\right) = \tan\left(\frac{\pi \gamma_P}{2}\right) \text{sgn}(\omega) \frac{\omega}{c_{\text{phase}}^P}$$
$$\alpha_S = -\omega \,\text{Im}\left(\frac{1}{V_S}\right) = \tan\left(\frac{\pi \gamma_S}{2}\right) \text{sgn}(\omega) \frac{\omega}{c_{\text{phase}}^S}. \quad (25)$$

Equations of motion in 2D space

Following is the wave equation in explicit form in the 2D case, considering the (x,z)-plane. From equations 1 and 17, I have

$$\partial_{tt}^2 u_1 = \rho^{-1}(\partial_1 \sigma_{11} + \partial_3 \sigma_{13} + f_1)$$
$$\partial_{tt}^2 u_3 = \rho^{-1}(\partial_1 \sigma_{13} + \partial_3 \sigma_{33} + f_3) \quad (26)$$

and

$$\sigma_{11} = C_{\mathcal{E}} D^{2\gamma_P}(\epsilon_{11} + \epsilon_{33}) - 2C_{\mu} D^{2\gamma_S} \epsilon_{33} + f_{11},$$
$$\sigma_{33} = C_{\mathcal{E}} D^{2\gamma_P}(\epsilon_{11} + \epsilon_{33}) - 2C_{\mu} D^{2\gamma_S} \epsilon_{11} + f_{33},$$
$$\sigma_{13} = 2C_{\mu} D^{2\gamma_S} \epsilon_{13} + f_{13}, \quad (27)$$

with

$$\epsilon_{11} = \partial_1 u_1,$$
$$\epsilon_{33} = \partial_3 u_3,$$
$$\epsilon_{13} = \frac{1}{2}(\partial_1 u_3 + \partial_3 u_1), \quad (28)$$

and I have introduced the moment-tensor components f_{11}, f_{33}, and f_{13}.

NUMERICAL ALGORITHM

I consider two explicit time-integration schemes to solve equations 26 and 27. They are based on the backward GL and CD fractional derivatives, which have first-order and second-order accuracy, respectively.

The GL fractional derivative of a function f is

$$h^{\nu} \frac{\partial^{\nu} f(t)}{\partial t^{\nu}} \sim \sum_{j=0}^{J} (-1)^j \binom{\nu}{j} f(t - jh), \quad (29)$$

where h is the time step, and $J = t/h - 1$. The derivation of this expression can be found, for instance, in Carcione et al. (2002).

On the other hand, the CD fractional derivative is given by

$$h^{\nu} \frac{\partial^{\nu} f(t)}{\partial t^{\nu}} \sim \sum_{j=0}^{J} (-1)^j \binom{\nu}{j} f\left[t - \left(j - \frac{\nu}{2}\right)h\right], \quad (30)$$

if ν is a quasi-even number, and

$$2h^{\nu} \frac{\partial^{\nu} f(t)}{\partial t^{\nu}} \sim \sum_{j=0}^{J} (-1)^j \binom{\nu}{j} \left(\frac{\nu - 2j + 1}{\nu - j + 1}\right) \times f\left[t - jh + \frac{h(\nu + 1)}{2}\right], \quad (31)$$

if ν is a quasi-odd number, as are the cases in the problem treated here. Equation 30 is a generalization of the usual CD formula, and equation 31 is derived in Appendix A. I assume these expressions in the fractional case, when ν is very close to odd and even numbers, i.e., $\nu \sim 1,3,5,\ldots$ and $\nu \sim 2,4,6,\ldots$, respectively. If ν is a natural number, I have the classical derivatives. In this case $J = \nu$ in equations 29 and 30, and $J = \nu + 1$ in equation 31. The GL and CD approximations are of order $O(h)$ and $O(h^2)$, respectively (Tuan and Gorenflo, 1995).

The fractional derivative of f at time t depends on all the previous values of f. This is the memory property of the fractional derivative,

related to field attenuation. The binomial coefficients are negligible for j exceeding an integer J. This allows truncation of the sum at $j = L, L \leq J$, where L is the effective memory length.

Fractional derivatives of order $2\gamma_P \ll 1$ and $2\gamma_S \ll 1$ require large memory resources and computational time because the decay of the binomial coefficients in equation 29 is slow (Carcione et al., 2002) and the effective memory length L is large. I increase the order of the derivative by applying a derivative of order m to equations 26 and 27. The exponent laws $D^m D^{2\gamma_P} = D^{m+2\gamma_P}$ and $D^m D^{2\gamma_S} = D^{m+2\gamma_S}$ hold in this case because of the initial data 2 and condition 3. The result is

$$D^{m+2}u_1 = \rho^{-1}(\partial_1 q_{11} + \partial_3 q_{13} + D^m f_1),$$
$$D^{m+2}u_3 = \rho^{-1}(\partial_1 q_{13} + \partial_3 q_{33} + D^m f_3) \qquad (32)$$

and

$$q_{11} = C_\mathcal{E}(\partial_1 D^\alpha u_1 + \partial_3 D^\alpha u_3) - 2C_\mu \partial_3 D^\beta u_3 + D^m f_{11},$$
$$q_{33} = C_\mathcal{E}(\partial_1 D^\alpha u_1 + \partial_3 D^\alpha u_3) - 2C_\mu \partial_1 D^\beta u_1 + D^m f_{33},$$
$$q_{13} = C_\mu(\partial_1 D^\beta u_3 + \partial_3 D^\beta u_1) + D^m f_{13}, \qquad (33)$$

where

$$\alpha = m + 2\gamma_P \text{ and } \beta = m + 2\gamma_S. \qquad (34)$$

It is enough to take $m = 1$ to have a considerable saving in memory storage compared to $m = 0$.

Time stepping based on the GL derivative

I discretize equations 32 and 33 at $t = nh$ with $m = 1$. For instance,

$$h^3(D^3u)^n = u^{n+1} - 3u^n + 3u^{n-1} - u^{n-2} \qquad (35)$$

and

$$h^\alpha(D^\alpha u)^n = u^n + \sum_{j=1}^{J} (-1)^j \binom{\alpha}{j} u^{n-j}, \qquad (36)$$

where I have used a right-shifted FD expression for the third derivative, which corresponds to replacing $t - jh$ by $t - (j-1)h$ in equation 29 (e.g., Gorenflo and Mainardi, 1998; Tadjeran and Meerschaert, 2007).

The time-stepping algorithm is as follows:

- Compute $(D^\alpha u_1)^n$, $(D^\alpha u_3)^n$, $(D^\beta u_1)^n$, and $(D^\beta u_3)^n$ using 36.
- Compute $(q_{11})^n$, $(q_{33})^n$, and $(q_{13})^n$ from 33.
- Compute the RHS of equation 32.
- Update the field variables $(n+1 \to n, n \to n-1, \ldots)$.
- Obtain u_1^{n+1} and u_3^{n+1} using equation 35 and repeat the algorithm.

Time-stepping based on the CD derivative

I discretize equation 32 at $t = nh$, with $m = 1$, using A-4 in Appendix A. For instance,

$$2h^3(D^3u)^n = u^{n+2} - 2u^{n+1} + 2u^{n-1} - u^{n-2}. \qquad (37)$$

The discretization of equation 33 makes use of A-4. For instance,

$$2h^\alpha(D^\alpha u)^n \sim u^{n+1} + \sum_{j=1}^{J} (-1)^j \binom{\alpha}{j} \times \left(\frac{\alpha - 2j + 1}{\alpha - j + 1}\right) u^{n-j+1}, \qquad (38)$$

where I have assumed that $u^{n-(2j-\alpha-1)/2} \sim u^{n-j+1}$ because $\alpha \sim 1$.

In this case, u^{n+2} is computed at each time step. The time-stepping algorithm is as follows:

- Compute $(D^\alpha u_1)^n$, $(D^\alpha u_3)^n$, $(D^\beta u_1)^n$, and $(D^\beta u_3)^n$ using 38.
- Compute $(q_{11})^n$, $(q_{33})^n$, and $(q_{13})^n$ from 33.
- Compute the RHS of equation 32.
- Obtain u_1^{n+2} and u_3^{n+2} using equation 37.
- Update the field variables $(n+1 \to n, n \to n-1, \ldots)$ and repeat the algorithm.

The spatial derivatives are calculated with the Fourier method by using the fast Fourier transform (FFT) (Kosloff and Baysal, 1982; Carcione, 2007). The Fourier pseudospectral method has spectral accuracy for band-limited signals (the approximation tends exponentially to the exact value). Then, the results are not affected by spatial numerical dispersion. In the case of inhomogeneous media, the algorithm employs the staggered Fourier method (Fornberg, 1996). Staggered operators evaluate derivatives between grid points. For instance, if Δx is the grid (cell) size and k_1 is the wavenumber component, a phase shift $\exp(\pm ik_1\Delta x/2)$ is applied when computing the x-derivative. Then, $\partial_1 \sigma^{-1} \partial_1$ is calculated as $D_1^- \sigma^{-1} D_1^+$, where $D_1^\pm$ is the discrete operator and $\pm$ refers to the sign of the phase shift. The spatial differentiation requires the interpolation of the material properties at half grid points. The method is given in detail in Appendix B.

SIMULATIONS

Attenuation measurements in a relatively homogeneous medium (Pierre Shale) were made by McDonal et al. (1958) near Limon, Colorado. They report a constant-Q behavior with attenuation $\alpha_P = 0.12f$ and $\alpha_S = 1.0f$ where α is given in dB per 1000 ft and the frequency f in Hz. I use SI units, such that 1 Np (neper) = 20/ln(10) dB and 1ft = 0.3048 m. Conversion of units implies α (dB/1000 ft) = $[\ln(10)/(20 \times 0.3048)]\,\alpha$ (Np/km) $\simeq 0.3778\,\alpha$ (Np/km). For low-loss solids, the quality factor is

$$Q = \frac{\pi f}{\alpha c},$$

with α given in nepers per unit length (Toksöz and Johnston, 1981). Because c_P and c_S are approximately 7100 ft/s (2164 m/s) and 2630 ft/s (802 m/s), the quality factors are $Q_P \simeq 32$ and $Q_S \simeq 10$. Then, $\gamma_P = 0.01$ and $\gamma_S = 0.03$. I consider a reference frequency $f_0 = \omega_0/(2\pi) = 100$ Hz, corresponding to the dominant frequency of the seismic source used in the experiments.

I evaluate the accuracy of the fractional derivatives by computing the FD phase velocity and attenuation factor in Appendix C. The P- and S-wave phase velocities and attenuation factors versus frequency $f = \omega/2\pi$ are shown in Figures 1 and 2, respectively, where the black squares represent the experimental data, the solid line is the exact value, and the dashed and dotted lines correspond to $m = 0$ and $m = 1$, using the CD fractional derivative. In both cases, the memory length is 70 and the time step is $h = 0.2$ ms. As can be seen, the $m = 1$ case is more accurate for the same memory length. In this case, the decay of the binomial coefficients in the series expansion is faster. This is illustrated in Figure 3, which shows the logarithm of the absolute value of the binomial coefficients versus the summation index. The GL derivative is the most used in fractional calculus. I use the CD derivative because of its better accuracy. The advantage of the first one is the fact that it can be used for any order of

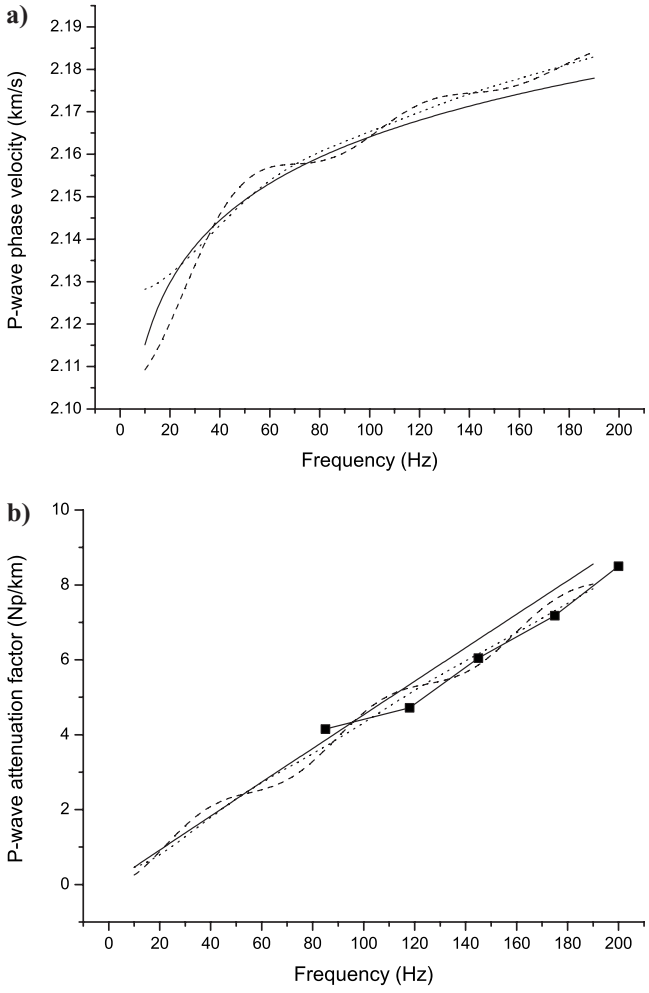

Figure 1. P-wave phase velocity (a) (equation 24) and attenuation factor (b) (equation 25) versus frequency in Pierre Shale (solid line) ($Q_P \simeq 30$ and $Q_S \simeq 10$). The dashed and dotted lines correspond to the CD fractional derivative with $m = 0$ and $m = 1$, respectively (calculated using equations C-3 and C-4). The memory length is 70. The squares represent the experimental data reported by McDonal et al. (1958).

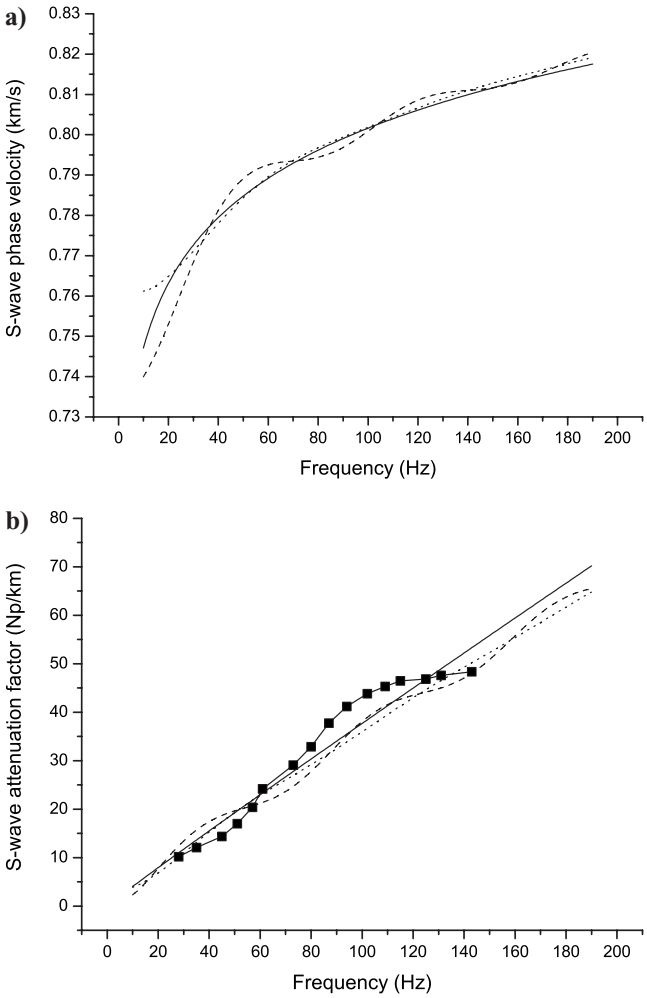

Figure 2. S-wave phase velocity (a) (equation 24) and attenuation factor (b) (equation 25) versus frequency in Pierre Shale (solid line). The dashed and dotted lines correspond to the CD fractional derivative with $m = 0$ and $m = 1$, respectively (calculated using equations C-3 and C-4). The memory length is 70. The squares represent the experimental data reported by McDonal et al. (1958).

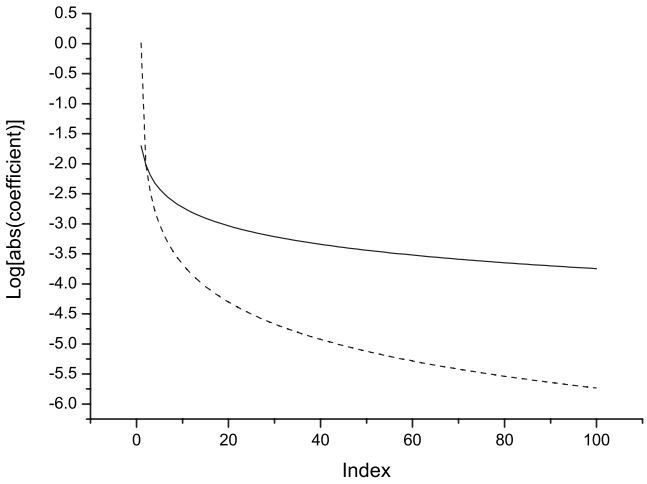

Figure 3. Decimal logarithm of the absolute value of the binomial coefficients versus the summation index for the CD approximation with $m = 0$ and $m = 1$ (solid and dashed lines). The order of the derivative is $m + 2\gamma_P$, with $\gamma_P = 0.01$.

the derivative, while the second one requires the order to be a quasi-odd or a quasi-even number. For the examples considered in this work, α and β are approximately equal to 1 (see equation 34).

The Pierre-Shale medium is discretized on a numerical mesh, with uniform vertical and horizontal grid spacings of 2 m, and 273 $\times$ 273 grid points. The source, applied at the center of the mesh, is a Ricker-type wavelet, whose amplitude spectrum is a Gaussian function centered at 100 Hz and an approximate cutoff frequency of 200 Hz. I use the CD fractional derivative, $m = 1$, a memory length of 40, and a time step $h = 0.2$ ms. I have found instabilities when using $m > 1$, i.e., fourth and higher time derivatives in equation 32. This problem also exists in the lossless case. However, the saving in computer memory is significant. As can be seen in Figure 3, I truncate the expansion at a value of nearly 10^{-5} for the absolute value of the binomial coefficients when using $m = 1$, whereas achieving the same precision with $m = 0$ gives a memory length of one more order of magnitude. Figure 4 represents snapshots of the vertical displacement in a lossless medium equivalent to Pierre Shale (4), and in the real (dissipative) model of Pierre Shale (4). The amplitudes in Figure 4b are 12 times weaker than in Figure 4a. The comparison shows that, as expected, the shear wave (inner wave) has been attenuated more than the compressional wave. A 2D analytical solution in a homogeneous medium is obtained in Appendix D. Figure 5 compares the analytical and numerical solutions of the horizontal (Figure 5a) and vertical (Figure 5b) displacements corresponding to Pierre Shale ($Q_P \simeq 32$ and $Q_S \simeq 10$).

Finally, I consider an example of seismic wave propagation in inhomogeneous media, in particular, a crosswell experiment. The geological model is shown in Figure 6, and the material properties are indicated in Table 1, where I have used the same reference frequency $f_0 = 45$ Hz for all the media. The low velocities and low quality factors of medium 4 simulate a highly porous, partially saturated sandstone. The medium is discretized with uniform vertical and horizontal grid spacings of 9 m, and 280 $\times$ 280 grid points. The constant-Q attenuation model is used to implement absorbing strips of width 50 grid points at the four boundaries of the mesh to avoid wraparound.

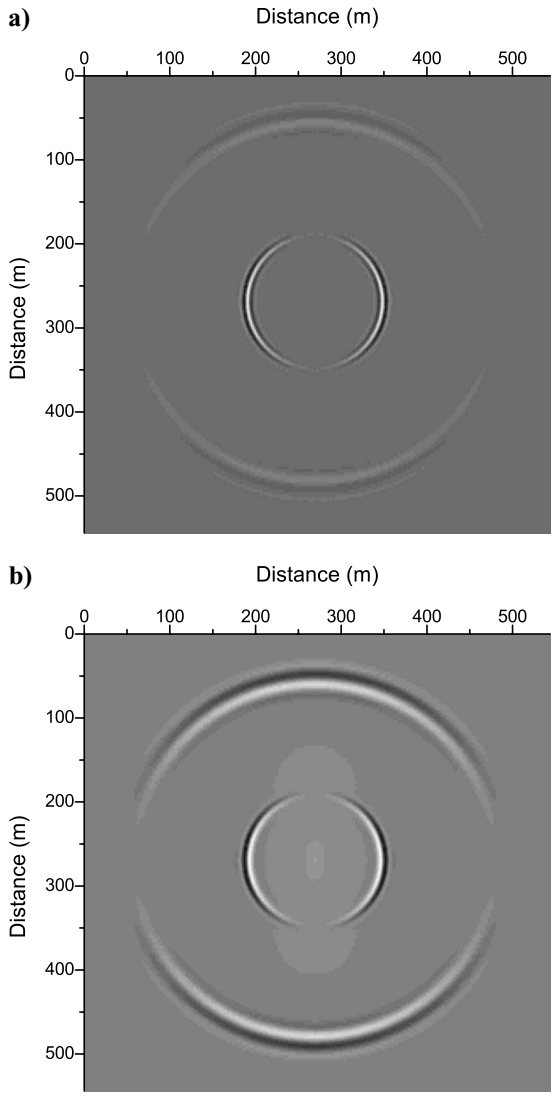

Figure 4. Snapshots at 125 ms of the vertical displacement in a lossless medium equivalent to Pierre Shale (a) and Pierre Shale ($Q_P \simeq 32$ and $Q_S \simeq 10$) (b). The plot in (b) has been rescaled with a gain factor of 12.

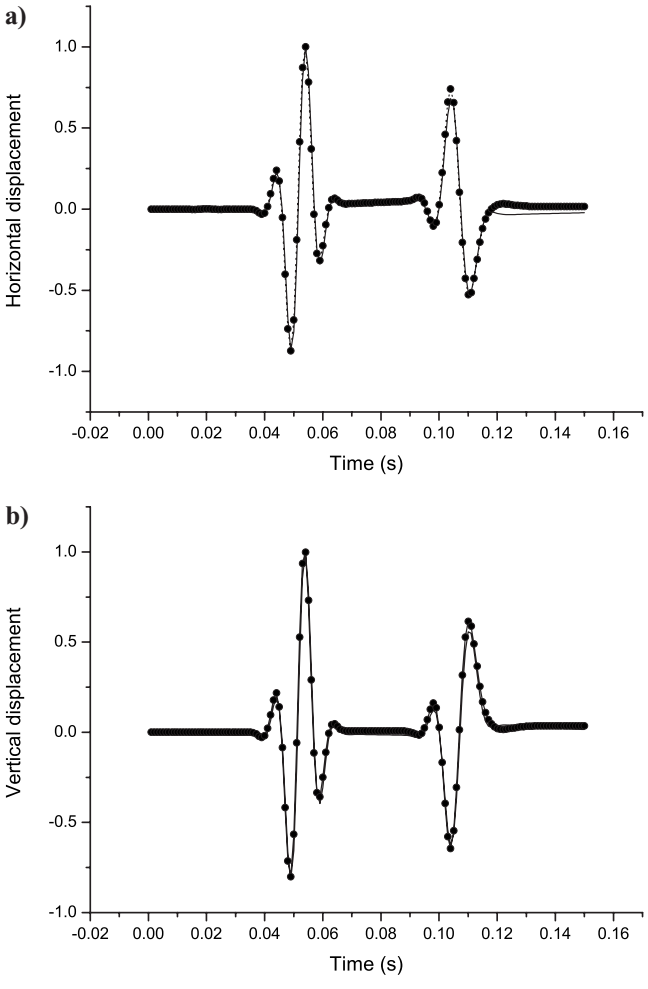

Figure 5. Seismograms in Pierre Shale corresponding to the horizontal (a) and vertical (b) displacements. Comparison between analytical and numerical solutions (solid and dotted lines) at $(x,z) = (50,50)$ m from the source.

The source is a horizontal force with Ricker-wavelet time history and a central frequency of 45 Hz, and the wavefield is computed by means of the CD approximation using a time step of 0.2 ms and a memory length $L = 40$. The synthetic seismograms recorded in the receiver well, corresponding to the lossless case and lossy case, are shown in Figure 7a and b, respectively, where the seismogram in Figure 7b has been rescaled with a gain factor of 1.83. The two main events are the direct P- and S-waves.

A similar hyperbolic power law that can also be implemented using fractional derivatives has been introduced by Hanyga and Seredyńska (2003), which has been tested in acoustic imaging (Ribodetti and Hanyga, 2004). Further research should be performed to avoid the memory storage implied by the numerical solution of the derivatives. For instance, Lu and Hanyga (2005) have used a new method for calculating the fractional derivative without storing and integrating the entire field histories.

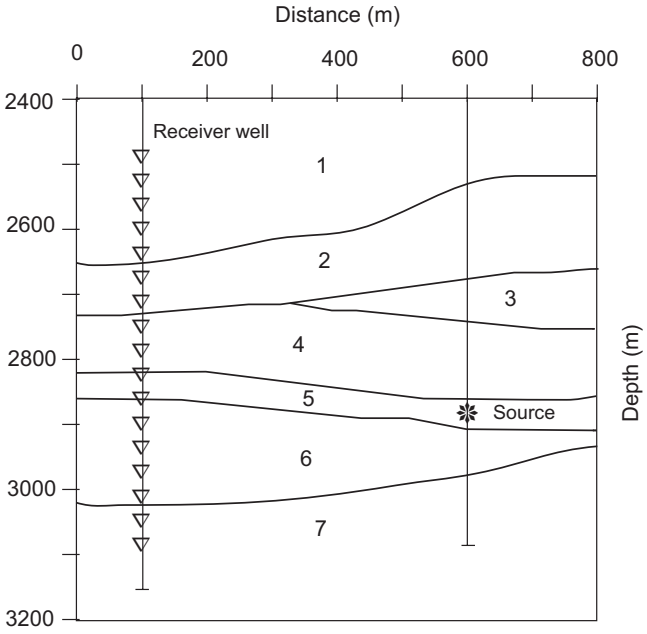

Figure 6. Geological model corresponding to a crosswell experiment. The properties of the model are given in Table 1.

Table 1. Reference wave velocities, density, and quality factors.

Medium	c_P (km/s)	c_S (km/s)	ρ (g/cm^3)	Q_P	Q_S
1	3.2	1.85	2.5	100	50
2	3.3	1.91	2.52	110	55
3	3.6	2.08	2.58	120	60
4	2.9	1.67	2.4	30	15
5	3.6	2.08	2.7	140	70
6	3.7	2.14	2.71	150	75
7	3.85	2.22	2.72	165	80

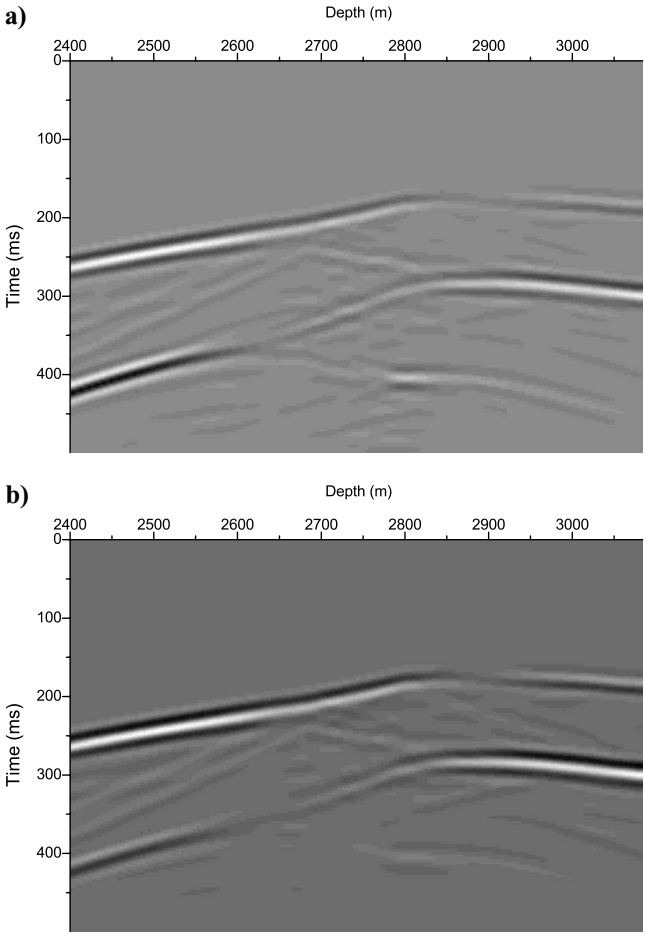

Figure 7. Lossless (a) and lossy (b) synthetic seismograms of the vertical displacement, corresponding to the model illustrated in Figure 6. The plot in (b) has been rescaled with a gain factor of 1.83.

CONCLUSIONS

The concept of fractional derivative has been used to simulate constant-Q wave propagation of P- and S-waves in the time domain using the classical power-law stress-strain relation widely used in seismology in the frequency domain. The equations are solved with the Grünwald-Letnikov and central-difference fractional derivatives for the time discretization and the Fourier method to compute the spatial derivatives. The validity and accuracy of the algorithm is verified by comparison with a 2D analytical solution in homogeneous media. The modeling in heterogeneous media is illustrated with a crosswell seismic experiment, where the seismograms show that, because of the lower S-wave Q factor, the direct shear wave has been attenuated more than the direct compressional wave. Then, the relative P/S amplitudes are greatly affected in the lossy (real) case.

Further research involves the extension to the 3D case and the improvement of the method by reducing or avoiding the memory storage implied by the numerical solution of the fractional derivatives. The key method is to transform the fractional derivative into an infinite integral over auxiliary internal variables. By approximating the integral using a specific quadrature formula, the derivative can be evaluated by solving ordinary differential equations for a finite set of quadrature nodes.

ACKNOWLEDGMENTS

I thank Associate Editor Deyan Draganov, Andrzej Hanyga, and two anonymous reviewers for their helpful comments.

APPENDIX A

CENTRAL-DIFFERENCE FRACTIONAL DERIVATIVE

The central-difference approximation to the derivative of order m (a natural number) is given by

$$h^m\frac{\partial^m f(t)}{\partial t^m}\sim\sum_{j=0}^{m}(-1)^j\binom{m}{j}f\left[t-\left(j-\frac{m}{2}\right)h\right], \tag{A-1}$$

where h is the time step. Note that the central difference has, for odd m, h multiplied by nonintegers. This can be solved by taking the average

$$2f\left[t-\left(j-\frac{m}{2}\right)h\right]\sim f\left[t-\left(j-\frac{m+1}{2}\right)h\right]+f\left[t-\left(j-\frac{m-1}{2}\right)h\right]. \tag{A-2}$$

Substituting this equation into A-1 yields

$$2h^m\frac{\partial^m f(t)}{\partial t^m}\sim f\left[t+\left(\frac{m+1}{2}\right)h\right]+\sum_{j=1}^{m+1}(-1)^j\left[\binom{m}{j}-\binom{m}{j-1}\right]f\left[t-\left(j-\frac{m+1}{2}\right)h\right]. \tag{A-3}$$

The binomial coefficients can be defined in terms of Euler's gamma function as

$$\binom{m}{j}=\frac{\Gamma(m+1)}{\Gamma(j+1)\Gamma(m-j+1)}$$

and can be calculated by a simple recursion formula

$$\binom{m}{j}=\frac{m-j+1}{j}\binom{m}{j-1},\quad\binom{m}{0}=1,$$

which also holds for a noninteger m. Using these properties, I obtain the following expression,

$$2h^\nu\frac{\partial^\nu f(t)}{\partial t^\nu}\sim\sum_{j=0}^{J}(-1)^j\binom{\nu}{j}\left(\frac{\nu-2j+1}{\nu-j+1}\right)\times f\left[t-jh+\frac{h(\nu+1)}{2}\right], \tag{A-4}$$

for a noninteger and quasi-odd ν. Note that this expression cannot be used for $\nu=m$ (integer) because it is singular for $j=m+1$.

There are no restrictions in the right-hand side of equations A-1 and A-4 that require m to be an integer. Replacing m by any positive real number ν gives the fractional-derivative approximation, provided that the two expressions are used for quasi-even and quasi-odd orders, respectively.

The extension of the upper limit from $m+1$ to $t/h-1$ has an important consequence. While in equations A-1 and A-4 the series has vanishing terms beyond $j=m$, in the fractional equations these terms are different from zero.

For more details on the theory and applications of fractional calculus, the reader is referred to Oldham and Spanier (1974), Gorenflo and Mainardi (1997), and Podlubny (1999).

APPENDIX B

STAGGERED FOURIER METHOD FOR THE FRACTIONAL WAVE EQUATION

On a regular grid the field components and material properties are represented at each grid point, say, represented by the symbol ♠, while on a staggered grid, variables and material properties are defined at half-grid points as indicated in the following mesh:

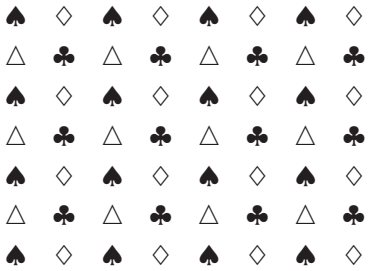

such that,

$$\begin{aligned}&\spadesuit(i,j)\sigma_{11},\sigma_{33},C_{\mathcal{E}},\alpha,\\&\diamondsuit\left(i+\frac{1}{2},j\right)v_1,f_1,\rho,\\&\triangle\left(i,j+\frac{1}{2}\right)v_3,f_3,\rho,\\&\clubsuit\left(i+\frac{1}{2},j+\frac{1}{2}\right)\sigma_{13},C_\mu,\beta.\end{aligned} \tag{B-1}$$

Material properties at half-grid points ♢, ♣, and △ are computed by averaging the values defined at regular points ♠. The averaging is chosen in such a way to reduce the error between the numerical solution corresponding to an interface aligned with the numerical grid and the equivalent solution obtained with a regular grid. Minimum ringing amplitudes are obtained when the averages are computed as follows. The density at points ♢ and △ as

$$\rho^{i+1/2,j}=\frac{1}{2}(\rho^{i,j}+\rho^{i+1,j}) \tag{B-2}$$

and

$$\rho^{i,j+1/2} = \frac{1}{2}(\rho^{i,j} + \rho^{i,j+1}), \tag{B-3}$$

respectively; C_μ at points ♣ as

$$(C_\mu^{i+1/2,j+1/2})^{-1} = \frac{1}{4}[(C_\mu^{i,j})^{-1} + (C_\mu^{i+1,j})^{-1} + (C_\mu^{i,j+1})^{-1} + (C_\mu^{i+1,j+1})^{-1}] \tag{B-4}$$

(Carcione, 1999); and β as a simple arithmetic averaging of the form

$$\beta^{i+1/2,j+1/2} = \frac{1}{4}(\beta^{i,j} + \beta^{i+1,j} + \beta^{i,j+1} + \beta^{i+1,j+1}). \tag{B-5}$$

The first-order derivative computed with the staggered differential operator is evaluated between grid points and uses even-based Fourier transforms. The standard first-order differential operator along the x-direction is

$$D_1\varphi = \sum_{k_1=0}^{k_1(N)} \mathrm{i}k_1\tilde{\varphi}(k_1)\exp(\mathrm{i}k_1x), \tag{B-6}$$

where $\tilde{\varphi}$ is the Fourier transform of φ and $k_1(N)$ is the Nyquist wavenumber. Staggered operators, that evaluate the derivatives between grid points, are given by

$$D_1^{\pm}\varphi = \sum_{k_1=0}^{k_1(N)} \mathrm{i}k_1 \exp(\pm\,\mathrm{i}k_1\Delta x/2)\tilde{\varphi}(k_1)\exp(\mathrm{i}k_1x), \tag{B-7}$$

where Δx is the grid spacing.

The staggered equations corresponding to 32 and 33 can be written as

$$\begin{aligned}
\diamond D^{m+2}u_1 &= \rho^{-1}(D_1^+q_{11} + D_3^-q_{13} + D^mf_1),\\
\triangle D^{m+2}u_3 &= \rho^{-1}(D_1^-q_{13} + D_3^+q_{33} + D^mf_3),\\
\spadesuit q_{11} &= C_{\mathcal{E}}(D_1^-D^\alpha u_1 + D_3^-D^\alpha u_3)\\
&\quad - 2C_\mu D_3^-D^\beta u_3 + D^mf_{11},\\
\spadesuit q_{33} &= C_{\mathcal{E}}(D_1^-D^\alpha u_1 + D_3^-D^\alpha u_3)\\
&\quad - 2C_\mu D_1^-D^\beta u_1 + D^mf_{33},\\
\clubsuit q_{13} &= C_\mu(D_1^+D^\beta u_3 + D_3^+D^\beta u_1) + D^mf_{13}.
\end{aligned} \tag{B-8}$$

APPENDIX C

FINITE-DIFFERENCE PHASE VELOCITY AND ATTENUATION FACTOR

I evaluate the accuracy of the time discretizations by computing the finite-difference phase velocity and attenuation factor and comparing them with the corresponding exact quantities (see Simulations section). Let us assume constant material properties, propagation along the x-direction and a field kernel $\exp(\mathrm{i}(\omega nh - kx)$, with $t = nh$ and k the complex horizontal wavenumber component (the complex velocity is given by ω/k). Substituting this kernel into equations 32 and 33 give the following complex velocities:

$$\bar{V}_{\mathrm{P}} = \mathrm{i}\theta\theta_0^{-\gamma_{\mathrm{P}}}\sqrt{\frac{\mathcal{E}_0a_\alpha}{\rho}}\exp(\mathrm{i}\theta/2), \tag{C-1}$$

and

$$\bar{V}_{\mathrm{S}} = \mathrm{i}\theta\theta_0^{-\gamma_{\mathrm{S}}}\sqrt{\frac{\mu_0a_\beta}{\rho}}\exp(\mathrm{i}\theta/2), \tag{C-2}$$

where $\theta = \omega h$, $\theta_0 = \omega_0 h$. The GL approximation has

$$a_\nu = \frac{\sum_{j=0}^{J}(-1)^j\binom{\nu}{j}\exp(-\mathrm{i}j\theta)}{\sum_{j=1}^{2+m}(-1)^j\binom{2+m}{j}\exp(-\mathrm{i}j\theta)},$$

where the D^{2+m} derivative has been right shifted (the term $\exp(\mathrm{i}\theta/2)$).

On the other hand, the CD approximation has the same a_ν of the GL approximation for even m, and

$$a_\nu = \frac{\sum_{j=0}^{J}(-1)^j\binom{\nu}{j}\left(\frac{\nu-2j+1}{\nu-j+1}\right)\exp(-\mathrm{i}j\theta)}{1+\sum_{j=1}^{3+m}(-1)^j\left[\binom{2+m}{j}-\binom{2+m}{j-1}\right]\exp(-\mathrm{i}j\theta)}$$

for odd m.

The finite-difference phase velocities are given by

$$\bar{c}^{\mathrm{P}}_{\mathrm{phase}} = \left[\mathrm{Re}\left(\frac{1}{\bar{V}_{\mathrm{P}}}\right)\right]^{-1} \text{ and } \bar{c}^{\mathrm{S}}_{\mathrm{phase}} = \left[\mathrm{Re}\left(\frac{1}{\bar{V}_{\mathrm{S}}}\right)\right]^{-1}, \tag{C-3}$$

whereas the attenuation factors are

$$\bar{\alpha}_{\mathrm{P}} = -\omega\,\mathrm{Im}\left(\frac{1}{\bar{V}_{\mathrm{P}}}\right) \text{ and } \bar{\alpha}_{\mathrm{S}} = -\omega\,\mathrm{Im}\left(\frac{1}{\bar{V}_{\mathrm{S}}}\right). \tag{C-4}$$

APPENDIX D

ANALYTICAL SOLUTION IN A 2-D HOMOGENEOUS MEDIUM

The solution of the wavefield generated by an impulsive point force in a 2-D elastic medium is given by Eason et al. (1956) (see also Pilant [1956]). For a force acting in the positive z-direction, this solution can be expressed as

$$u_1(r,t) = \left(\frac{F_0}{2\pi\rho}\right)\frac{xz}{r^2}[G_1(r,t) + G_3(r,t)], \tag{D-1}$$

$$u_3(r,t) = \left(\frac{F_0}{2\pi\rho}\right)\frac{1}{r^2}[z^2 G_1(r,t) - x^2 G_3(r,t)], \tag{D-2}$$

where F_0 is a constant that gives the magnitude of the force, $r = (x^2 + z^2)^{1/2}$,

$$G_1(r,t) = \frac{1}{c_P^2}(t^2 - \tau_P^2)^{-1/2}H(t - \tau_P) + \frac{1}{r^2}(t^2 - \tau_P^2)^{1/2}H(t - \tau_P) - \frac{1}{r^2}(t^2 - \tau_S^2)^{1/2}H(t - \tau_S) \tag{D-3}$$

and

$$G_3(r,t) = -\frac{1}{c_S^2}(t^2 - \tau_S^2)^{-1/2}H(t - \tau_S) + \frac{1}{r^2}(t^2 - \tau_P^2)^{1/2}H(t - \tau_P) - \frac{1}{r^2}(t^2 - \tau_S^2)^{1/2}H(t - \tau_S), \tag{D-4}$$

$$\tau_P = \frac{r}{c_P}, \quad \tau_S = \frac{r}{c_S}, \tag{D-5}$$

and c_P and c_S are the compressional- and shear-wave phase velocities. To apply the correspondence principle and obtain the anelastic solution, one needs the elastic frequency-domain solution (Bland, 1960; Carcione et al., 1988; Carcione, 2007). Using the transform pairs of the zero- and first-order Hankel functions of the second kind,

$$\int_{-\infty}^{\infty} \frac{1}{\tau^2}(t^2 - \tau^2)^{1/2}H(t - \tau)\exp(i\omega t)dt = \frac{i\pi}{2\omega\tau}H_1^{(2)}(\omega\tau). \tag{D-6}$$

$$\int_{-\infty}^{\infty} (t^2 - \tau^2)^{-1/2}H(t - \tau)\exp(i\omega t)dt = -\frac{i\pi}{2}H_0^{(2)}(\omega\tau). \tag{D-7}$$

I obtain

$$u_1(r,\omega,c_P,c_S) = \left(\frac{F_0}{2\pi\rho}\right)\frac{xz}{r^2}[\widetilde{G}_1(r,\omega,c_P,c_S) + \widetilde{G}_3(r,\omega,c_P,c_S)], \tag{D-8}$$

$$u_3(r,\omega,c_P,c_S) = \left(\frac{F_0}{2\pi\rho}\right)\frac{1}{r^2}[z^2\widetilde{G}_1(r,\omega,c_P,c_S) - x^2\widetilde{G}_3(r,\omega,c_P,c_S)], \tag{D-9}$$

where

$$\widetilde{G}_1(r,\omega,c_P,c_S) = -\frac{i\pi}{2}\left[\frac{1}{c_P^2}H_0^{(2)}\left(\frac{\omega r}{c_P}\right) + \frac{1}{\omega r c_S}H_1^{(2)}\left(\frac{\omega r}{c_S}\right) - \frac{1}{\omega r c_P}H_1^{(2)}\left(\frac{\omega r}{c_P}\right)\right], \tag{D-10}$$

$$\widetilde{G}_3(r,\omega,c_P,c_S) = \frac{i\pi}{2}\left[\frac{1}{c_S^2}H_0^{(2)}\left(\frac{\omega r}{c_S}\right) - \frac{1}{\omega r c_S}H_1^{(2)}\left(\frac{\omega r}{c_S}\right) + \frac{1}{\omega r c_P}H_1^{(2)}\left(\frac{\omega r}{c_P}\right)\right]. \tag{D-11}$$

Using the correspondence principle, I replace the elastic wave velocities in D-8 and D-9 by the anelastic wave velocities V_P and V_S defined in equation 21. The 2-D viscoelastic Green's function can then be expressed as

$$u_1(r,\omega) = \begin{cases} u_1(r,\omega,V_P,V_S), & \omega \geq 0, \\ u_1^*(r,-\omega,V_P,V_S), & \omega < 0, \end{cases} \tag{D-12}$$

and

$$u_3(r,\omega) = \begin{cases} u_3(r,\omega,V_P,V_S), & \omega \geq 0, \\ u_3^*(r,-\omega,V_P,V_S), & \omega < 0, \end{cases} \tag{D-13}$$

where the asterisk denotes complex conjugate. This frequency-domain form ensures that the solution is real in the time domain. Multiplication with the source time function and a numerical inversion by the discrete Fourier transform yield the desired time-domain solution ($\widetilde{G}_1$ and $\widetilde{G}_3$ are assumed to be zero at $\omega = 0$ because the Hankel functions are singular).

REFERENCES

Auld, B. A., 1990, Acoustic fields and waves in solids, Vol. 1: Robert E. Krieger, Publishing Co.

Bland, D. R., 1960, The theory of linear viscoelasticity: Pergamon.

Caputo, M., and F. Mainardi, 1971, Linear models of dissipation in anelastic solids: Rivista Il Nuovo Cimento (Ser. II), **1**, 161–198.

Carcione, J. M., 1999, Staggered mesh for the anisotropic and viscoelastic wave equation: Geophysics, **64**, 1863–1866.

———, 2007, Wave fields in real media. Theory and numerical simulation of wave propagation in anisotropic, anelastic, porous and electromagnetic media: Elsevier.

Carcione, J. M., F. Cavallini, F. Mainardi, and A. Hanyga, 2002, Time-domain seismic modeling of constant Q-wave propagation using fractional derivatives: Pure and Applied Geophysics, **159**, no. 7, 1719–1736.

Carcione, J. M., D. Kosloff, and R. Kosloff, 1988, Wave propagation simulation in a linear viscoelastic medium: Geophysical Journal of the Royal Astronomical Society, **95**, 597–611.

Christensen, R. M., 1982, Theory of viscoelasticity: Academic Press.

Eason, J., J. Fulton, and I. N. Sneddon, 1956, The generation of waves in an infinite elastic solid by variable body forces: Philosophical Transaction of the Royal Society of London, **A248**, 575–607.

Fellah, Z. E. A., and C. Depollier, 2000, Transient acoustic wave propagation in rigid porous media: A time-domain approach: Journal of the Acoustical Society of America, **107**, 683–688.

Fornberg, B., 1996, A practical guide to pseudospectral methods: Cambridge University Press.

Gorenflo, R., 1997, Fractional calculus, some numerical methods, *in* A. Carpinteri. and F. Mainardi, eds., Fractals and fractional calculus in continuum mechanics: Springer-Verlag, 277–290.

Gorenflo, R., and F. Mainardi, 1997, Fractional calculus: Integral and differential equations of fractional order, *in* A. Carpinteri. and F. Mainardi. eds., Fractals and fractional calculus in continuum mechanics: Springer-Verlag, 223–276.

———, 1998, Random walk models for space-fractional diffusion processes: Fractional Calculus & Applied Analysis, **1**, 167–191.

Grünwald, A. K., 1867, Über "begrenzte" Derivationen und deren Anwend-

ung: Zeitschrift für Angewandte Mathematik und Physik, **12**, 441–480.
Gurevich, B., and S. L. Lopatnikov, 1995, Velocity and attenuation of elastic waves in finely layered porous rocks: Geophysical Journal International, **121**, 933–947.
Hanyga, A., 2002, Multidimensional solutions of time-fractional diffusion-wave equations: Proceedings of the Royal Society of London, **A458**, 933–957.
Hanyga, A., and M. Seredyńska, 2003, Power law attenuation in acoustic and isotropic anelastic media. Geophysical Journal International, **155**, 830–838.
Kjartansson, E., 1979, Constant *Q*-wave propagation and attenuation: Journal of Geophysical Research, **84**, 4737–4748.
Kosloff, D., and E. Baysal, 1982, Forward modeling by the Fourier method: Geophysics, **47**, 1402–1412.
Letnikov, A. V., 1868, Theory of differentiation of fractional order: Matematiceskij Sbornik, **3**, 1–68 (in Russian).
Lu, J.-F., and A. Hanyga, 2005, Wave field simulation for heterogeneous porous media with singular memory drag force: Journal of Computational Physics, **208**, 651–674.
Mainardi, F., and M. Tomirotti, 1997, Seismic pulse propagation with constant *Q* and stable probability distributions: Annali di Geofisica, **40**, 1311–1328.
McDonal, F. J., F. A. Angona, R. L. Mills, R. L. Sengbush, R. G. Van Nostrand, and J. E. White, 1958, Attenuation of shear and compressional waves in Pierre Shale: Geophysics, **23**, 421–439.
Oldham, K. B., and J. Spanier, 1974, The fractional calculus: Academic Press.
Pilant, W. L., 1979, Elastic waves in the earth: Elsevier Publishing Company.
Podlubny, I., 1999, Fractional differential equations: Academic Press.
Ribodetti, A., and A. Hanyga, 2004, Some effects of the memory kernel singularity on wave propagation and inversion in viscoelastic media, II: Inversion: Geophysical Journal International, **158**, 426–442.
Scott-Blair, G. W., 1949, Survey of general and applied rheology: Pitman.
Tadjeran, M., and M. Meerschaert, 2007, A second-order accurate numerical method for the two-dimensional fractional diffusion equation: Journal of Computational Physics, **220**, 813–823.
Toksöz, M. N., and D. H. Johnston, 1981, Seismic wave attenuation, SEG.
Tuan, V. K., and R. Gorenflo, 1995, Extrapolation to the limit for numerical fractional differentiation: Zeitschrift für Angewandte Mathematik und Mechanik, **75**, 646–648.